

A Model Study of the Salish Sea Estuarine Circulation*

DAVID A. SUTHERLAND⁺ AND PARKER MACCREADY

School of Oceanography, University of Washington, Seattle, Washington

NEIL S. BANAS

Applied Physics Laboratory, University of Washington, Seattle, Washington

LUCY F. SMEDSTAD

Naval Research Laboratory, Stennis Space Center, Mississippi

(Manuscript received 2 August 2010, in final form 4 February 2011)

ABSTRACT

A realistic hindcast simulation of the Salish Sea, which encompasses the estuarine systems of Puget Sound, the Strait of Juan de Fuca, and the Strait of Georgia, is described for the year 2006. The model shows moderate skill when compared against hydrographic, velocity, and sea surface height observations over tidal and subtidal time scales. Analysis of the velocity and salinity fields allows the structure and variability of the exchange flow to be estimated for the first time from the shelf into the farthest reaches of Puget Sound. This study utilizes the total exchange flow formalism that calculates volume transports and salt fluxes in an isohaline framework, which is then compared to previous estimates of exchange flow in the region. From this analysis, residence time distributions are estimated for Puget Sound and its major basins and are found to be markedly shorter than previous estimates. The difference arises from the ability of the model and the isohaline method for flux calculations to more accurately estimate the exchange flow. In addition, evidence is found to support the previously observed spring–neap modulation of stratification at the Admiralty Inlet sill. However, the exchange flow calculated increases at spring tides, exactly opposite to the conclusion reached from an Eulerian average of observations.

1. Introduction

This study aims to understand the processes controlling the salt content in Puget Sound, Washington, a large fjord estuarine system located in the northeastern Pacific (Fig. 1). Puget Sound is connected to the coastal ocean via the Strait of Juan de Fuca (SJdF), a 200-km-long, 20-km-wide, 200-m-deep strait that collects the freshwater exported by not only Puget Sound but the Strait of Georgia (SoG) to the north as well. The region as a whole is known as the Salish Sea.

Puget Sound has characteristics of a partially mixed estuary, despite its fjord-like geometry, most notably an along-estuary salinity gradient ($\sim 2 \times 10^{-5}$ psu m^{-1}) that drives a strong exchange flow. The exchange flow at the Admiralty Inlet (AIN) sill, located near the entrance to Puget Sound, has been estimated as $10\text{--}20 \times 10^3$ m^3 s^{-1} , about 10–20 times the average river flow into Puget Sound (Cokelet et al. 1991; Babson et al. 2006). This exchange flow was observed to vary on spring–neap time scales because of variations in the strength of tidal mixing (Geyer and Cannon 1982), a process also observed at the entrance to the SoG (Griffin and LeBlond 1990; Masson and Cummins 2000). The amplification of transport into and out of Puget Sound decreases the residence time of waters there from 5 yr, which is the freshwater filling time based on river flow alone, to a range of 90–180 days that is based on a two-layer box model approach (Babson et al. 2006). This difference in residence times, as well as understanding the processes that control the exchange and mixing of oceanic and freshwater, is critical across the Salish Sea as environmental issues such as hypoxia,

* Ecology and Oceanography of Harmful Algal Blooms Program Contribution Number 635, and Pacific Northwest Toxins Program Contribution Number 4.

⁺ Current affiliation: NOAA/Northwest Fisheries Science Center, Seattle, Washington.

Corresponding author address: David A. Sutherland, NOAA/Northwest Fisheries Science Center, 2725 Montlake Blvd. E, Seattle, WA 98112.
E-mail: david.sutherland@noaa.gov

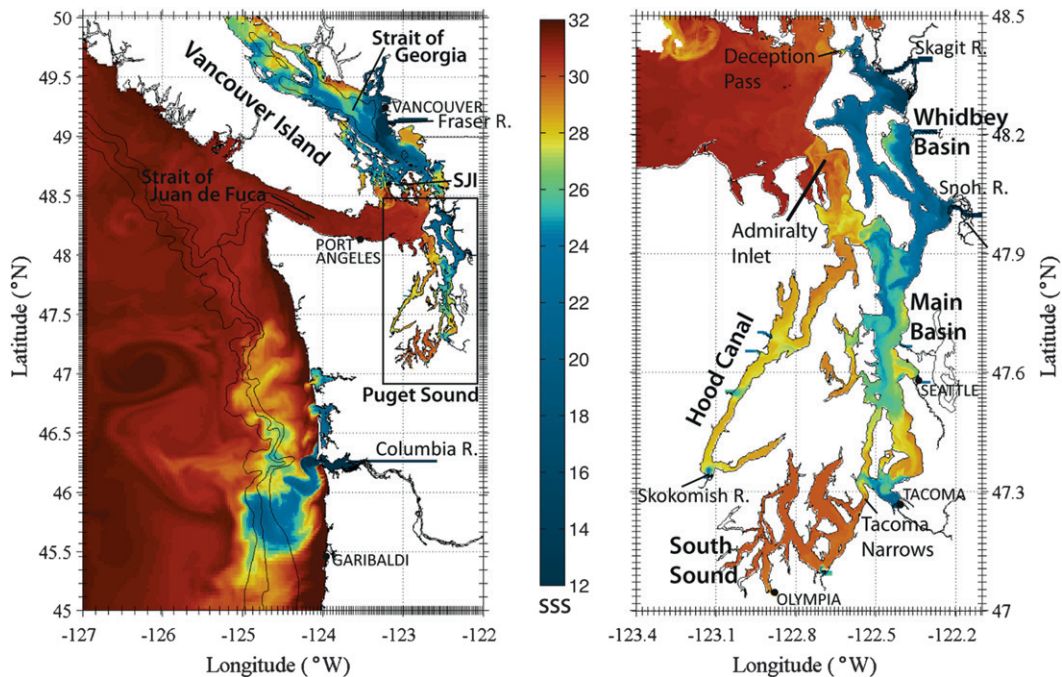


FIG. 1. (left) A model snapshot of sea surface salinity on 21 Jun 2006, several days after the onset of coastal upwelling, overlaid on a regional map showing the model domain and main geographical features. Black lines depict the 200-, 500-, and 1000-m isobaths. (right) Zoom in on Puget Sound [boxed region in (left)] showing the major basins, rivers, and sill regions mentioned in the text. Dashes along each axis show every fourth point of the stretched model grid.

pollution, and the threat of oil spills continue to be of concern (e.g., Newton et al. 2007).

Sills also connect two of the major basins inside Puget Sound, Hood Canal (HCN) to Main Basin (MB; Gregg and Pratt 2010) and South Sound to Main Basin (through Tacoma Narrows; Seim and Gregg 1997), whereas Whidbey Basin, the site of the largest rivers in Puget Sound, has no sill restricting its flow to Main Basin. The numerous headlands in the region generate internal waves and eddies that act as a drag on the tidal flow and provide energy to mixing processes. For example, at Three Tree Point in southern Main Basin, the form drag due to flow past the headland is estimated to be 10–50 times that because of bottom drag alone (Edwards et al. 2004; McCabe et al. 2006).

Although numerous observational programs have studied the SJdF, Puget Sound, and the coastal ocean of the Pacific Northwest, none has attempted to cover the entire region at once. The present study is the first to ask how the Salish Sea as a whole functions as an estuary. We use a newly developed numerical model of the Salish Sea that depends heavily on previous observational programs to validate and interpret the model results. The next section outlines the model setup and forcing.

We then present model–data comparisons, which show that the model has moderate skill. Observations taken during the River Influences on Shelf Ecosystems (RISE) project (Hickey et al. 2010) and from other sources in the

Salish Sea, such as the Ecology and Oceanography of Harmful Algal Blooms Pacific Northwest (ECOHAB-PNW) project, form the basis for the model–data comparisons. In section 4, we explore the variability in the salt content of Puget Sound by calculating the exchange flow and corresponding salt flux through a number of cross sections using an isohaline framework (MacDonald 2006). The level of detail made possible by the combination of the new model and the isohaline exchange flow analysis leads to markedly shorter estimates of the residence times compared to previous studies. It also provides a new view of the dynamics in this system, challenging the prevailing notion that the exchange flow increases during neap tides at Admiralty Inlet. Finally, it allows one to examine the distribution of freshwater from different river sources to the estuary, showing that about half of the Skagit River discharge exits through Deception Pass (DP), instead of southward through the main passage of Whidbey Basin (WBN).

2. Model configuration

a. Model grid and parameters

We use the Regional Ocean Modeling System (ROMS; Rutgers version 3), a free-surface, hydrostatic, primitive equation model that has been used extensively in both coastal (e.g., Zhang et al. 2009) and estuarine systems (e.g.,

Warner et al. 2005; MacCready et al. 2009). The horizontal grid encompasses the Salish Sea and extends southward to 45°N and offshore to 127°W, ranging in resolution from a minimum of 280 m inside Puget Sound to a maximum of 3.1 km in the southeastern corner (Fig. 1). The model has 20 terrain-following sigma coordinate layers with stretching parameters chosen that result in twice the vertical resolution in the upper 20% of the water column ($\theta_s = 4$, $\theta_b = 0.5$, and $h_c = 0$). The minimum depth was set to 4 m to avoid drying of grid cells. Bathymetry data came from a global 2-min gridded dataset (Smith and Sandwell 1997), which was overlaid with a 250-m resolution Cascadia dataset where available (Haugerud 2000), and finally a Puget Sound-only digital elevation model (PSDEM 2005; Finlayson 2005) with a resolution of 183 m. The bathymetry was smoothed to decrease the numerical errors that occur near steeply sloping bathymetry, a common feature of the fjords in the Salish Sea. Maximum $r_0 \sim 0.4$ ($r_0 = |\Delta h|/h$, where h is water depth; e.g., Beckmann and Haidvogel 1993), whereas the stiffness number (Haney 1991) $r_1 \sim 9$.

Turbulence closure is given by the k - ϵ version of the generic length scale (GLS) formulation (Umlauf and Burchard 2003), using values suggested by Warner et al. (2005) and the Canuto-A stability functions (Canuto et al. 2001). Previous realistic hindcast simulations of the Columbia River region showed that these choices improved overall model skill (MacCready et al. 2009; Liu et al. 2009b). Background values of the vertical viscosity and diffusivity were set to $5 \times 10^{-6} \text{ m}^2 \text{ s}^{-1}$, a small constant horizontal diffusion of tracers was used with diffusivity equal to $2 \text{ m}^2 \text{ s}^{-1}$, and no explicit horizontal diffusion of velocity was used. Bottom stress was parameterized with a quadratic drag law with a coefficient $C_d = 3 \times 10^{-3}$ and a no-slip condition along the horizontal boundaries. Results from sensitivity experiments where the horizontal diffusion of tracers was varied from 1 to $5 \text{ m}^2 \text{ s}^{-1}$ and from experiments where C_d was varied by two orders of magnitude were not significantly different than those presented below. ROMS was run using the default, third-order upstream advection scheme for velocity and a recursive 3D advection scheme [Multi-dimensional Positive Definite Advection Transport Algorithm (MPDATA)] for tracers. The model was run for a year starting on 1 January 2006, with a baroclinic time step of 30 s with 20 fast barotropic time steps. Output files were written once per hour.

b. Boundary conditions and model initialization

The Salish Sea model is one-way nested inside the global Navy Coastal Ocean Model (NCOM), a data-assimilative model that has a nominal resolution of $1/8^\circ$ (Barron et al. 2006, 2007). Initial fields for salinity S and

temperature T were taken from NCOM on 1 January 2006 and interpolated onto the model grid. Because global NCOM does not extend into Puget Sound, we modified the initial fields of T and S inside Puget Sound by utilizing available CTD observations taken in December 2005 [Puget Sound Regional Synthesis Model (PRISM) cruise; see section 3b]. At every model grid point, the closest T and S profiles from the CTD stations were used to extrapolate horizontally and fill the Puget Sound initial condition. A similar method was used to initialize the T and S fields inside the Strait of Georgia, where, again, the global NCOM model does not cover. In that case, initial fields were based on CTD profiles obtained from the Canadian Institute of Ocean Sciences (IOS) database for a week before and after 1 January 2006. Initial fields of velocity u and v and sea surface height ζ were set to zero everywhere.

At the southern and western open boundaries, the model fields (T , S , u , v , and ζ) are relaxed to NCOM values (subsampled to every 2 days) over a 6-gridpoint-wide region. Time scales for the nudging are 3 days at each boundary, increasing to 60 days at 6 grid points in. Radiation conditions are used on all model fields at the boundary, whereas open boundary conditions for the free-surface and depth-averaged momentum are given by the Chapman (1985) and Flather (1976) formulations, respectively. The northern boundary in the Strait of Georgia was closed.

c. Rivers, tides, and atmospheric forcing

The model includes 16 rivers, simulated as point sources at the end of uniform depth river channels. Because the river channels were not explicitly resolved in making the grid, they were carved out and set to depths ranging from 4 to 12 m. Daily river discharge and temperature time series for the model are taken from corresponding U.S. Geological Survey (USGS) gauging stations and an Environment Canada gauging station in Hope, British Columbia, for the Fraser River. The Columbia River was the largest source of freshwater (Fig. 2), with a double-peaked discharge with a maximum $\sim 13\,000 \text{ m}^3 \text{ s}^{-1}$, followed by the Fraser River that peaks in midsummer near $7000 \text{ m}^3 \text{ s}^{-1}$. The combined Skagit and Snohomish river system dominates Puget Sound with a maximum discharge of $\sim 7000 \text{ m}^3 \text{ s}^{-1}$ and a mean of $1000 \text{ m}^3 \text{ s}^{-1}$.

Tidal forcing was imposed on top of the slowly varying climatology fields at the open boundaries using eight constituents (M_2 , S_2 , K_1 , O_1 , N_2 , P_1 , K_2 , and Q_1) derived from the $1/4^\circ$ TPXO7.1 inverse global tidal model (Egbert and Erofeeva 2002). Tides in the PNW are often mixed semidiurnal, with pronounced spring-neap variability and diurnal inequalities (e.g., Fig. 3). Tidal amplitude

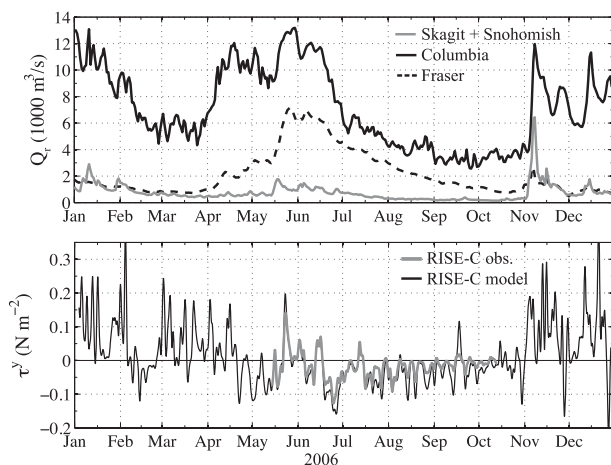


FIG. 2. (top) Daily time series of observed river discharge Q_r ($1000 \text{ m}^3 \text{ s}^{-1}$) during 2006 for the Columbia, Fraser, and the combined Skagit and Snohomish rivers. (bottom) North-south wind stress τ^y (N m^{-2}) used in the model at the central RISE mooring location, where $\tau^y < 0$ indicates upwelling favorable winds. The gray line shows the observed wind stress at the same location, available only during the summer and early fall.

generally increases landward, growing to $>3 \text{ m}$ in South Sound (Mojfeld and Larsen 1984).

Meteorological fields of surface pressure, 10-m winds, 2-m temperature, 2-m relative humidity, shortwave radiation, and downward longwave radiation were derived from two versions of the Northwest Modeling Consortium fifth-generation Pennsylvania State University-National Center for Atmospheric Research Mesoscale Model (MM5) regional forecast model (Mass et al. 2003). A 4-km resolution, hourly output MM5 model covers the majority of the model domain, from 126° to 111°W and from 41.5° to 49.5°N . Outside of that region, a 12-km version of the MM5 model extended the spatial coverage of the atmospheric fields. The meteorological fields are subsampled to every 4 h for use in ROMS. The ROMS model uses bulk flux parameterizations to derive surface momentum and heat fluxes to the ocean from the atmosphere (Fairall et al. 1996). The model wind stress correlates well with the observed winds taken from a surface buoy outside the Columbia River mouth during the summer of 2006 (Fig. 2; Tinis et al. 2006). The wind record shows the dominant seasonality observed in the Salish Sea region, with upwelling favorable winds (southward) common in the summer, whereas strong, storm-driven winds prevail during the fall and winter months.

3. Model validation: Comparison with observations

Model validation is done by quantifying comparisons against observations and by defining and interpreting appropriate model skill scores (e.g., Willmott 1981;

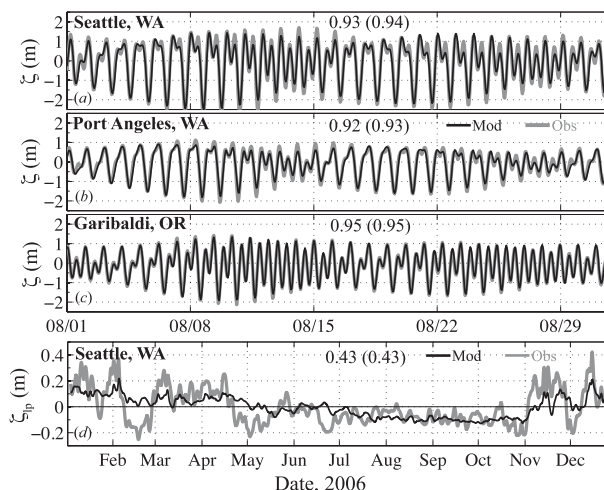


FIG. 3. (a)–(c) Time series of sea surface height ζ (m) measured by NOAA tide gauges (gray) and simulated by the model (black) for a month-long period in the summer of 2006. Skill scores are listed for each location, with correlation coefficients R^2 listed in parentheses. All R^2 were significant at the 95% level. (d) A year-long record of the observed subtidal sea surface height ζ_{ip} (m) recorded at the Seattle, Washington, tide gauge (gray) plotted against the modeled ζ_{ip} (black).

Murphy 1988; Oke et al. 2002; Warner et al. 2005; Wilkin 2006). We choose to use a combination of two commonly used metrics: the first is the correlation coefficient R^2 , which is the covariance between two variables and equals

$$R = \frac{1}{\sigma_m} \frac{1}{\sigma_o} \frac{1}{N} \sum_{i=1}^N (m_i - \bar{m})(o_i - \bar{o}), \quad (3.1)$$

where m_i is the model variable at time or location i ; o_i is the observed variable at time or location i ; N is the number of observations; σ_m and σ_o are the standard deviations of the model and observed variables, respectively; and the overbar indicates an average. The statistical significance of the correlation coefficient (at the 95% level) is based on the effective degrees of freedom, which is calculated as $N' - 2$, where N' is the e -folding value of the autocovariance of the observed variable (Emery and Thomson 1997). For records with small N , such as the repeat CTD stations discussed below, we use Student's t test to determine if the correlation is significant.

A skill score SS for a model is generally defined as $SS = 1 - X/X_{\text{ref}}$, where X is a model-data comparison statistic and the subscript ref refers to a reference experiment (e.g., Murphy 1988; Ralston et al. 2010). Positive SS means the new run performs better than the reference run, whereas negative SS indicates worse

TABLE 1. Skill scores SS of sea surface height ζ comparisons between the model and nine NOAA tide gauges over 2006. Correlation coefficients R^2 are reported in parentheses. The remaining columns show the amplitude ratio A_r of modeled to observed amplitudes and the difference in phase (relative to UTC) θ_d of the modeled minus observed phases for three select tidal constituents.

Location	SS (R^2)	M_2		S_2		K_1	
		A_r	θ_d	A_r	θ_d	A_r	θ_d
Astoria, OR	0.85 (0.86)	0.83	21°	0.84	22°	0.96	13°
Garibaldi, OR	0.95 (0.95)	0.99	5.4°	1.1	5.9°	0.99	0.5°
La Push, WA	0.90 (0.91)	0.94	12°	0.91	13°	0.98	4.2°
Neah Bay, WA	0.94 (0.95)	0.89	7.9°	0.85	10°	0.97	2.9°
Port Angeles, WA	0.92 (0.93)	0.69	13°	0.70	12°	1.0	0.6°
Port Townsend, WA	0.94 (0.94)	0.75	-14°	0.75	12°	1.0	-2.5°
Friday Harbor, WA	0.92 (0.92)	0.86	25°	0.83	25°	1.0	-3.3°
Seattle, WA	0.93 (0.94)	0.75	12°	0.76	9.9°	1.0	-3.7°
Tacoma, WA	0.93 (0.94)	0.75	12°	0.76	9.3°	1.0	-3.6°

performance. We use a skill score with $X = \text{MSE}$ as the second validation metric. MSE is a measure of the difference between the model and observed quantities and has dimensional units, and it equals

$$\text{MSE} = \frac{1}{N} \sum_{i=1}^N (m_i - o_i)^2. \quad (3.2)$$

Here, SS is the combination of three terms, $\text{SS} = R^2 - \text{VB} - \text{MB}$, where VB is a bias error associated with the variance (i.e., not getting the amplitude of the variable correctly) and MB is a mean bias error. Thus, in all cases, $\text{SS} < R^2$.

a. Sea surface height

Observed records of ζ come from nine available National Oceanic and Atmospheric Administration (NOAA) tide gauges (<http://tidesandcurrents.noaa.gov/>) located around the region (Table 1). The model captures the amplitude, phase, and spring–neap variability of the tidal signals (Fig. 3), with $\text{SS} > 0.9$ everywhere and significant R^2 at all locations (Table 1). Ratios of the modeled to observed amplitudes of the M_2 , S_2 , and K_1 constituents, calculated using the T-TIDE analysis software in MATLAB (Pawlowicz et al. 2002), show that the model has better skill at diurnal frequencies (Table 1). At semi-diurnal frequencies, the modeled amplitude was generally too low. No tide gauge records are available in the farthest reaches of Puget Sound, such as South Sound or Hood Canal. However, comparisons of ζ against an empirical tide model tuned explicitly for Puget Sound (Lavelle et al. 1988) were statistically significant within each of these separate basins (not shown).

The range of the tidally averaged sea surface height, ζ_{lp} , was ~ 0.5 m inside Puget Sound, with low ζ_{lp} values during the upwelling season in the summer months. All tidal averaging is done with a Godin-type filter of consecutive 24–24–25 h running averages (Godin 1991). The

modeled subtidal variability was similar at all nine tide gauges and compared reasonably well with the observed ζ_{lp} , indicating the large spatial coherence of ζ_{lp} . The largest error was an event in February, which caused a low ζ_{lp} anomaly that was missed in the model. The model does not include an inverse barometer effect, so these errors are most likely caused by weather-induced pressure anomalies.

b. CTD comparisons

Profiles of T and S obtained from CTD casts are available from a number of sources throughout the Salish Sea region, with a total of 441 casts for 2006. The twice-yearly PRISM cruises gathered >40 profiles in both June and December 2006, whereas the Washington State Department of Ecology (DoE) monitors a series of repeat CTD locations in each of the major basins of Puget Sound (Fig. 4). In addition, the Joint Effort to Monitor the Strait (JEMS) program conducts regular CTD profiling at three stations south of the San Juan Islands (Fig. 4). CTD casts on the shelf come from the RISE project, with the majority clustered in water depths less than 200 m but with good coverage north and south around the RISE moorings. In the Strait of Georgia, as well as the channels of the San Juan Islands, CTD profiles taken in 2006 were obtained from the IOS database.

To quantitatively compare the model T and S profiles to the synoptic CTD casts, we first interpolated the observations and model profiles vertically onto a uniform depth grid with 1-m spacing. Next, we calculated a density profile $\rho(z)$ and defined the water column as stratified if the criteria $d\rho/dz < -0.1 \text{ kg m}^{-4}$ was met below a depth of 5 m (Moore et al. 2008). The depth of the maximum density gradient Z_s was calculated for each stratified CTD profile. We calculated the approximate two-layer stratification ΔS by taking the difference between the mean S of the lower ($z > Z_s$) and upper ($z < Z_s$) layers ($\Delta S > 0$ is stable). In cases categorized as unstratified, we define ΔS to be the water column difference in S . Figure 5 illustrates this method for

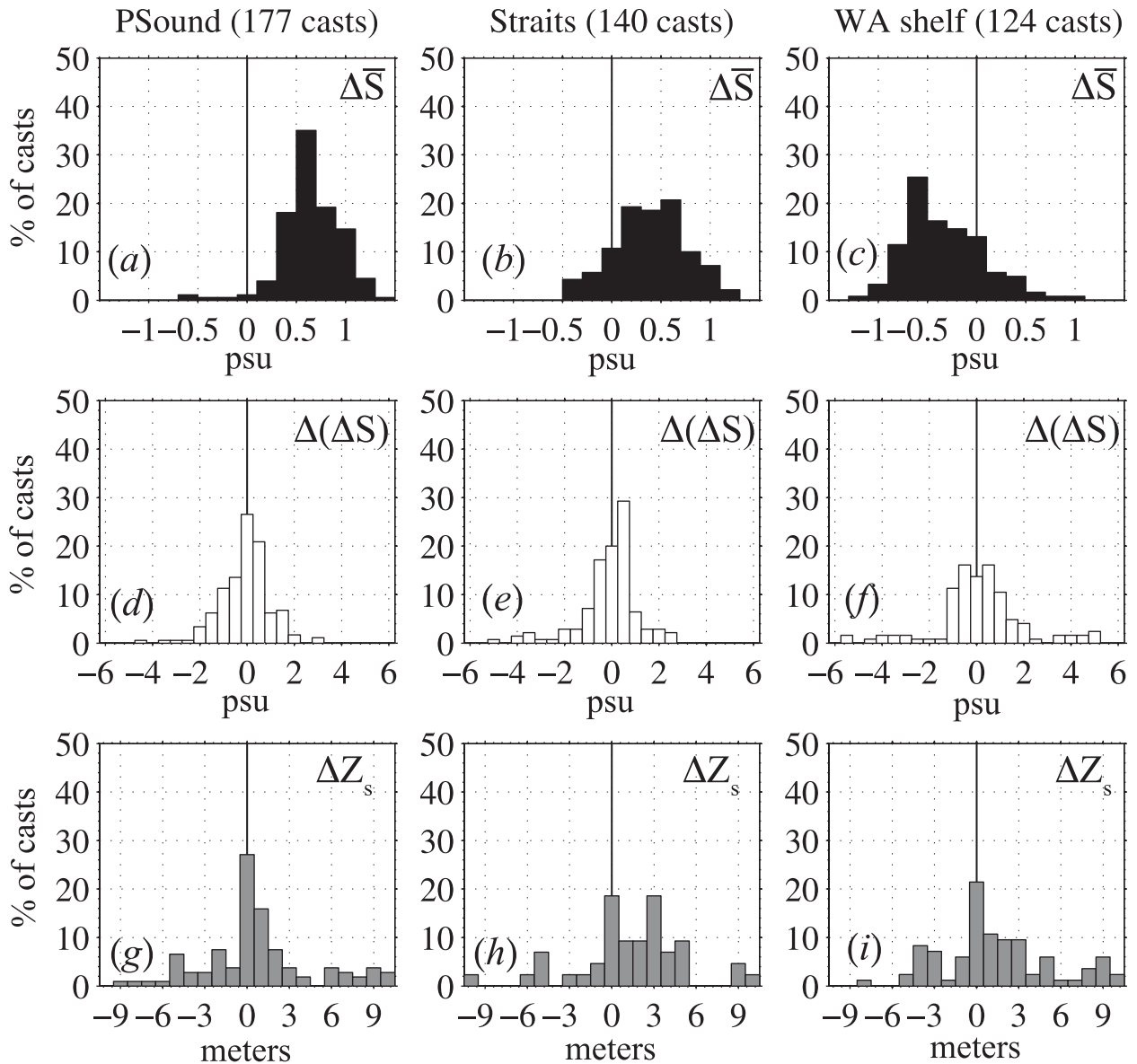


FIG. 6. (a)–(c) Histograms (percentage of total CTD casts) of $\Delta\bar{S}$ (psu) grouped by region, Puget Sound, the SJdF and SoG, and off of coastal Washington and the Columbia River. Here, $\Delta\bar{S}$ is the difference between the observed and modeled mean S . (d)–(f) As in (a)–(c), but for $\Delta(\Delta S)$ (psu), which is the mismatch between the difference of the top and bottom layer salinities of the model and observations. (g)–(i) As in (a)–(c), but for $|\Delta Z_s|$ (m), which is the difference in pycnocline depths measured observationally and calculated by the model. Note that the Straits region was commonly unstratified.

three areas: Puget Sound, coastal Washington (which includes any cast seaward of the Strait of Juan de Fuca), and the straits (SJdF and SoG). Histograms of the differences in mean S ($\Delta\bar{S}$), stratification [$\Delta(\Delta S)$], and Z_s (ΔZ_s), reveal significant biases that differ across each region (Fig. 6). In Puget Sound and the Straits, $\bar{S}_{\text{mod}} > \bar{S}_{\text{obs}}$ by ~ 0.5 psu, whereas, on the shelf, the model is too fresh ($\bar{S}_{\text{obs}} > \bar{S}_{\text{mod}}$) by a similar magnitude, ~ 0.5 psu. The model does better in capturing the salinity stratification inside Puget Sound, with mean differences in

ΔS near 0 but is overstratified slightly in the straits. Stratification is created by the influx of river water, which decreases S in the surface layer (Figs. 5a,c), as well as surface heating during the summer. Note that a majority of the straits' CTD profiles were located in the SJdF and the San Juan Islands and were unstratified (93 out of a total 140 casts). This reduced the number of casts in Fig. 6h, resulting in a $\Delta(\Delta S)$ statistic that mostly represents biases in top-to-bottom salinity differences (Fig. 6e). The ΔZ_s are clustered near zero in each region,

TABLE 2. Skill scores SS at repeat CTD stations (Washington DoE or JEMS). Correlation coefficients R^2 are reported in parentheses, with the difference commonly caused by the mean bias MB. Numbers in bold are $SS > 0$ and significant R^2 values at the 95% level. Numbers next to the station name indicate the number of casts taken in 2006.

Station	Surface S	Surface T	Deep S	Deep T
ADM001 (7)	0.73 (0.75)	0.67 (0.92)	-0.13 (0.60)	0.39 (0.53)
ADM002 (9)	0.18 (0.32)	0.21 (0.37)	0.19 (0.91)	0.22 (0.37)
PSB003 (8)	0.31 (0.72)	-0.34 (0.95)	0.88 (0.98)	0.98 (0.99)
SAR003 (11)	0.71 (0.83)	0.80 (0.94)	-3.1 (0.78)	0.92 (0.93)
MB-South (12)	0.40 (0.66)	0.76 (0.95)	-0.99 (0.69)	0.78 (0.87)
HCN (9)	-2.8 (0.51)	-0.89 (0.79)	0.79 (0.88)	-1.0 (0.16)
SSound (12)	-1.3 (0.64)	0.96 (0.98)	-1.1 (0.78)	0.98 (0.98)
JEMS-N (7)	0.14 (0.89)	0.86 (0.98)	0.87 (0.94)	0.42 (0.61)

though they are skewed toward positive values. This is another indication that the model stratification is too gradual and does not capture the sharp S and T gradients observed.

To examine the model's performance over seasonal time scales, we use the CTD observations from the available repeat stations (Fig. 4 and Table 2). At each station, we compare a surface (5 m deep) and deep (5 m from the bottom) T and S value against the model (Fig. 7). The T record clearly shows that the model captures the seasonal cycle of warming in the surface layer at both locations. In the deep layer, the Main Basin station exhibits warming through the fall, lagging the surface heating, whereas the JEMS-N deep T shows little variation. For all four T records shown, $SS > 0.4$, with significant R^2 values.

The seasonal trends in S are more difficult to interpret from monthly CTD casts, as freshwater input varies on much shorter time scales. However, S generally increases throughout the summer, in response to the prevailing upwelling conditions at the coast and the low-discharge conditions of local rivers (Fig. 2). The model-data comparisons are generally good, with $SS > 0$ and significant R^2 , with the one exception at the deep MB station. The model mean S is too salty there, decreasing SS to below zero, even though the R^2 value is significant.

Overall, the best model skill was located in the SJdF (JEMS-N), with significant R^2 and high SS in all variables (Table 2). The location with the worst overall performance was inside Hood Canal, where only the deep S showed better skill than the mean of the observations. However, the R^2 values were mostly significant, so the errors in Hood Canal came from a T/S mean bias. Hood Canal is one of the narrowest and deepest parts of Puget Sound, making it difficult to model accurately after bathymetric smoothing takes place. Even though grid resolution is on the order of 400 m there, there are sections that have <10 grid points across the channel.

c. Moored T/S comparisons

A more comprehensive view of the seasonal cycle, as well as short-term variability, comes from moored time series of T and S . Inside Puget Sound, the available mooring records for 2006 are scarce, with the only data obtained through the Hood Canal Dissolved Oxygen Program (HCDOP), which maintains a series of profiling moorings at several locations in Hood Canal. To complement the data inside Puget Sound, we also present comparisons with observations taken by the RISE project. In summer 2006, RISE maintained three shelf moorings that recorded T and S at 2 and 20 m, as well as full water column velocities from a bottom-mounted ADCP (Fig. 3).

The simulated S on the shelf at the RISE-N location (Fig. 8 and Table 3) shows the variability in the position of the Columbia River plume, which oscillates northward and southward, depending on the wind direction (García-Berdeal et al. 2002; Liu et al. 2009a). Low S events occur throughout the year, even during the summertime upwelling season, and the model does fairly well at capturing the timing and magnitude of these events. The model is too fresh at 20 m during the late summer. At the Hood Canal site, the S variability is smaller in magnitude and differs from the shelf in that the two dominant modes of variability occur at spring-neap and seasonal time scales. The model captures this S variability well in the surface layer but is offset by ~ 0.5 psu in the deep layer at 60 m.

The T comparisons (Figs. 8e-h) display a seasonal warming superimposed on plume-induced changes at the RISE-N site, and a small spring-neap variability in Hood Canal. The model surface warming is too strong in Hood Canal compared to the observations, which decreases SS there, despite a high R^2 .

d. Velocity comparisons

Accurately simulating the salinity structure of the Salish Sea is not enough to calculate salt fluxes; one needs the velocity field as well. Inside the SJdF, a strong estuarine circulation exists with a fresh surface outflow overlying a deeper, saltier inflow, with an estimated magnitude of 0.1–0.2 Sv (1 Sv $\equiv 10^6$ m³ s⁻¹; Labrecque et al. 1994; Thomson et al. 2007). Local winds drive the flow on the inner shelf that leads to upwelling conditions and also influence the propagation of the Columbia River plume, often times resulting in plumes in two directions of different ages (Hickey et al. 2009).

Figure 9 shows comparisons of modeled and observed tidally averaged currents at four locations around the region. At the mouth of the SJdF (EH1), the surface currents are directed westward at ~ 0.2 m s⁻¹ above 50 m, whereas deeper waters flow inward (Fig. 9e). Reversals

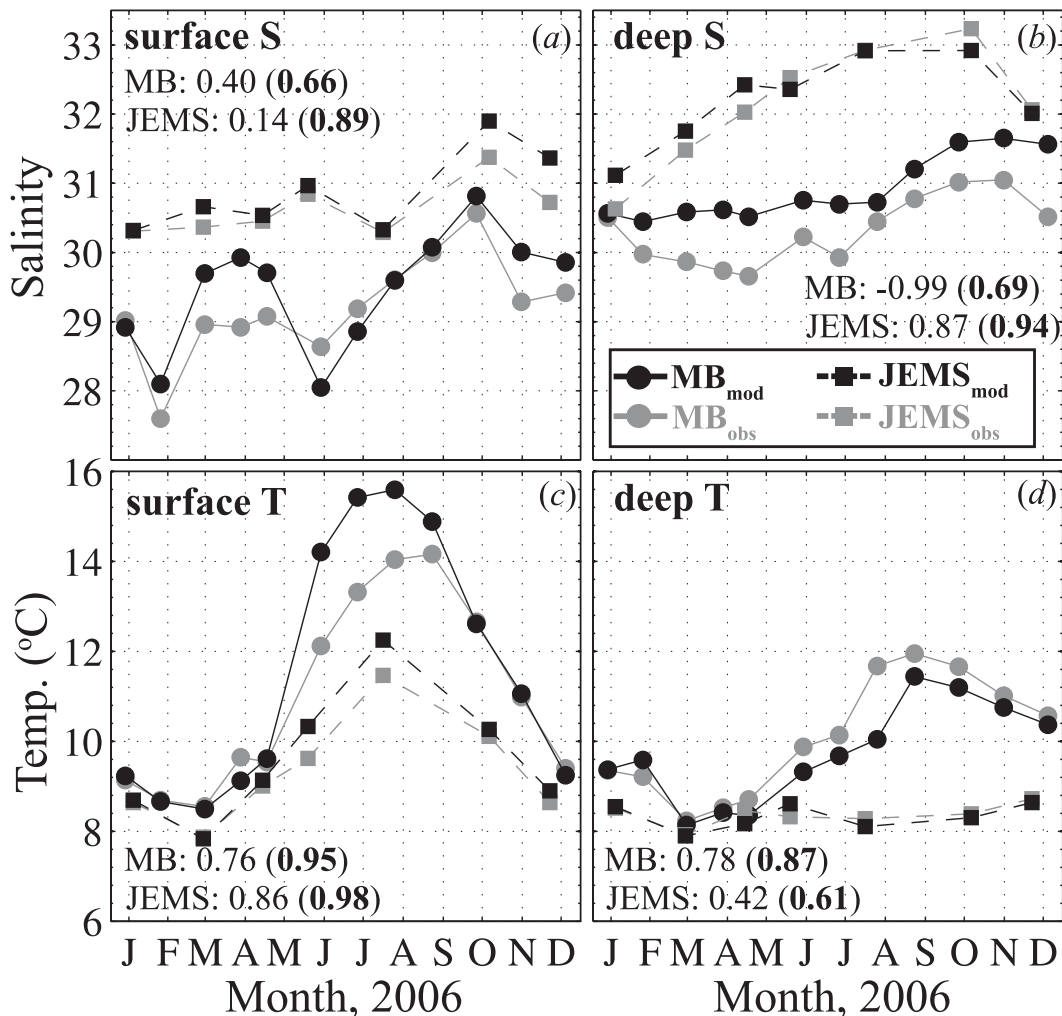


FIG. 7. (a) Observed (gray) and modeled (black) salinity time series taken at two repeat CTD stations at a depth of 5 m [MB south (solid line with circles); JEMS north (dashed line with squares)]. Skill scores SS are listed with R^2 correlation coefficients in parentheses (boldface if significant at the 95% level). (b) As in (a), but for deep salinity taken at a depth of 5 m off the bottom (183 m for MB south and 160 m for JEMS north). (c) As in (a), but for surface temperature (5 m). (d) As in (b), but for deep temperature.

in this estuarine like flow occur during all times of year (e.g., Frisch et al. 1981), with the variability captured only modestly by the model. The mean surface outflow speed is underestimated, resulting in $SS < 0$, despite a significant R^2 of 0.53. Table 4 lists SS and R^2 for all the current meter records available during 2006, with statistics for tidally averaged surface velocities u_{surf} and v_{surf} , tidally averaged deep velocity v_{deep} (u_{deep} for EH1), and depth-averaged velocities u_{ave} and v_{ave} .

The structure of $u(z)$ in the dominant east–west direction at EH1 is captured well. In the deep inflowing layer u_{deep} , however, the model does not reflect the amplitude of variability observed, resulting in a low SS.

At the RISE-N location, the model captures the response of the v_{surf} and v_{deep} currents over periods greater

than weekly, although it does a poorer job on the sub-weekly coastally trapped wave (CTW) time scales. The model overpredicts the mean $v(z)$ by 0.05 m s^{-1} (Fig. 9f), though the vertical shear is correct. The comparisons are similar at the RISE-S location, although the model $v(z)$ underpredicts the southward flow (Fig. 9g). The absence of weekly variability is consistent with the experience of Liu et al. (2009b) in modeling this shelf with the global NCOM boundary conditions. This would be a clear target for improvement to address scientific issues dependent on CTWs but is probably less important for studying the exchange flow in the Salish Sea.

Inside Hood Canal, the model is less successful at representing $v(z)$ (Fig. 9). The tidal currents are significantly correlated, although the variance in the model u_{ave}

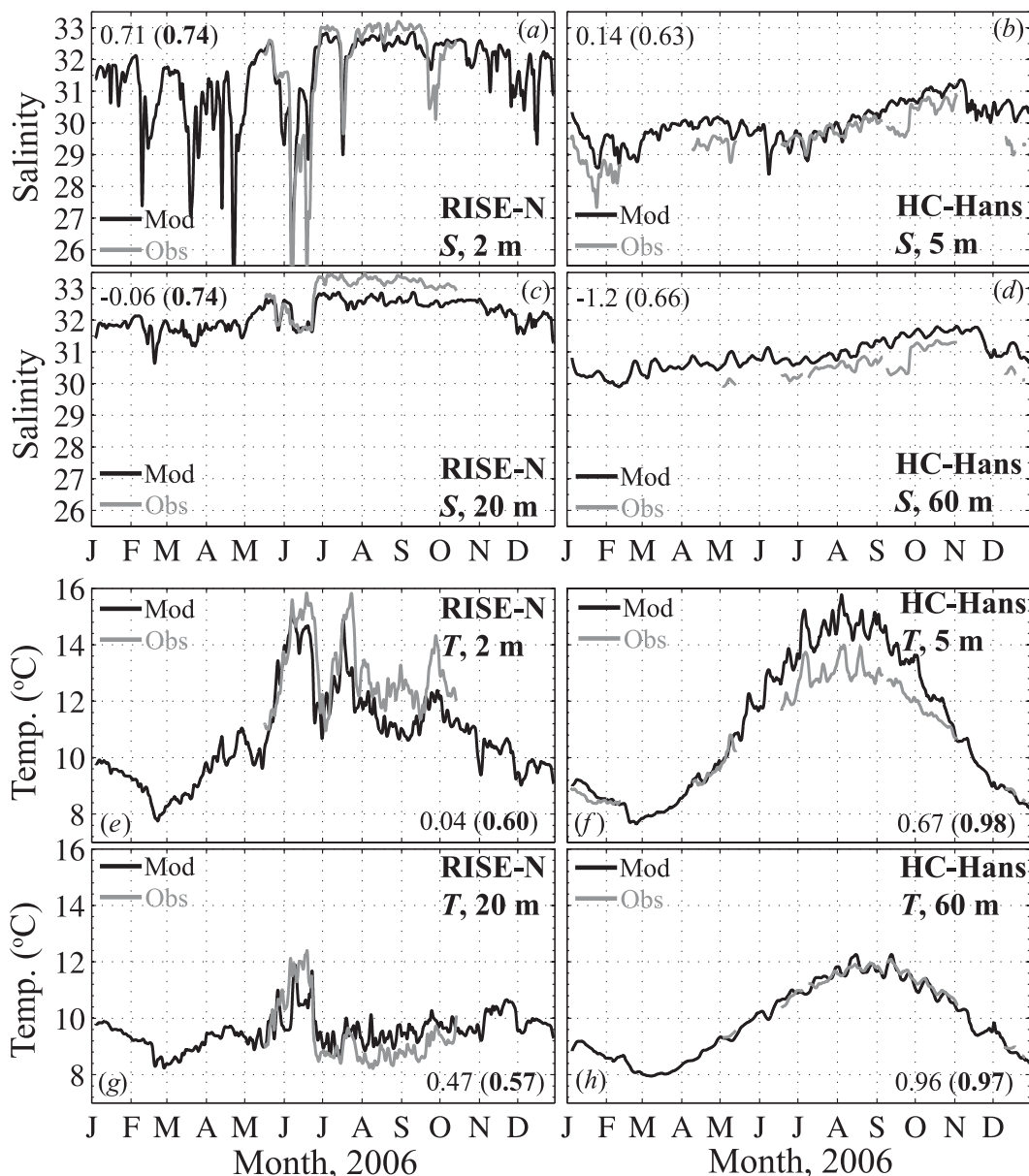


FIG. 8. (a)–(d) Observed (gray) and modeled (black) tidally averaged salinity time series at two depths at the RISE north location and two depths at the Hood Canal–Hansville mooring location. Skill scores SS are listed with R^2 correlation coefficients in parentheses (bold if significant at the 95% level). (e)–(h) As in (a)–(d), but for tidally averaged temperature time series.

is too small. The model shows a strongly sheared layer in the upper few meters that is not observed. This shallow upper layer may be missed by the observations, which were taken by an upward-looking, bottom-mounted ADCP, resulting in part of the error. A compensating southward flow is observed at a depth of ~ 10 m, but this inflow is spread over a greater depth in the model, with a peak magnitude centered at 20 m.

e. Model validation summary

The model performs adequately over a wide range of scales. It has well-developed estuarine flow in the SJdF, so the main mechanism controlling water properties in the Salish Sea appears to be functioning. Salinity structure in Puget Sound has roughly the right stratification and halocline depth but is too salty by about 0.5. One may infer from these that the exchange flow may be

TABLE 3. Skill scores SS and correlation coefficients R^2 for comparisons between moored temperature and salinity records and ROMS model output at various locations. The R^2 values for the time series that are significant at the 95% level are listed in bold, as are SS > 0 (for all comparisons).

Station	S_{surf}	T_{surf}	S_{deep}	T_{deep}
RISE-N	0.71 (0.74)	0.04 (0.60)	-0.06 (0.74)	0.47 (0.57)
RISE-C	0.01 (0.25)	0.49 (0.53)	0.10 (0.58)	-0.13 (0.17)
RISE-S	0.61 (0.61)	0.39 (0.42)	0.64 (0.74)	0.54 (0.68)
HCN-Hans	0.14 (0.63)	0.67 (0.98)	-1.2 (0.66)	0.96 (0.97)
HCN-Duck	-3.5 (0.73)	0.71 (0.84)	-1.2 (0.94)	-8.6 (0.46)
HCN-Hood	-0.42 (0.72)	0.85 (0.89)	-0.43 (0.86)	-0.67 (0.48)

about right but that the length of the model salt intrusion is too great. This deficiency may be due to poor resolution of topographic features that drive mixing (Edwards et al. 2004) and is discussed further in section 5. The annual cycle of surface and deep temperature and salinity are in reasonable agreement with observations. Moreover, these patterns have substantially higher correlation coefficients than those in the simplified box model of Babson et al. (2006, their Table 2). Thus it appears that the vastly greater complexity of the present model brings some benefits.

4. Results

The seasonal trend in salt content is similar across Puget Sound (Fig. 10). From the end of summer through the fall, Puget Sound gains salt with S increasing from 28.5 to 29.5 over a span of 3 months. During winter, the sound freshens rapidly, with the fastest and largest changes found in Whidbey Basin, where S drops from 29 to 27 in less than 2 weeks. Early spring brings an increase in salinity, followed by a relatively steady period until early summer, consistent with the trends seen in the monthly DoE (Fig. 7) and HCDOP data (Fig. 8). These three distinct time periods characterize all the Puget Sound regions. The most landward reaches, South Sound and Whidbey Basin, are generally the freshest throughout the year, whereas Admiralty Inlet is the saltiest. Admiralty Inlet and Whidbey Basin show the strongest nonseasonal variability, with pronounced changes on spring-neap time scales.

To characterize the estuarine nature of Puget Sound, we need to understand what controls the gain or loss of salt over a year. For example, when the region begins to gain salt, is it due to decreasing river discharge or to the increasingly saltier water in the SJdF after the onset

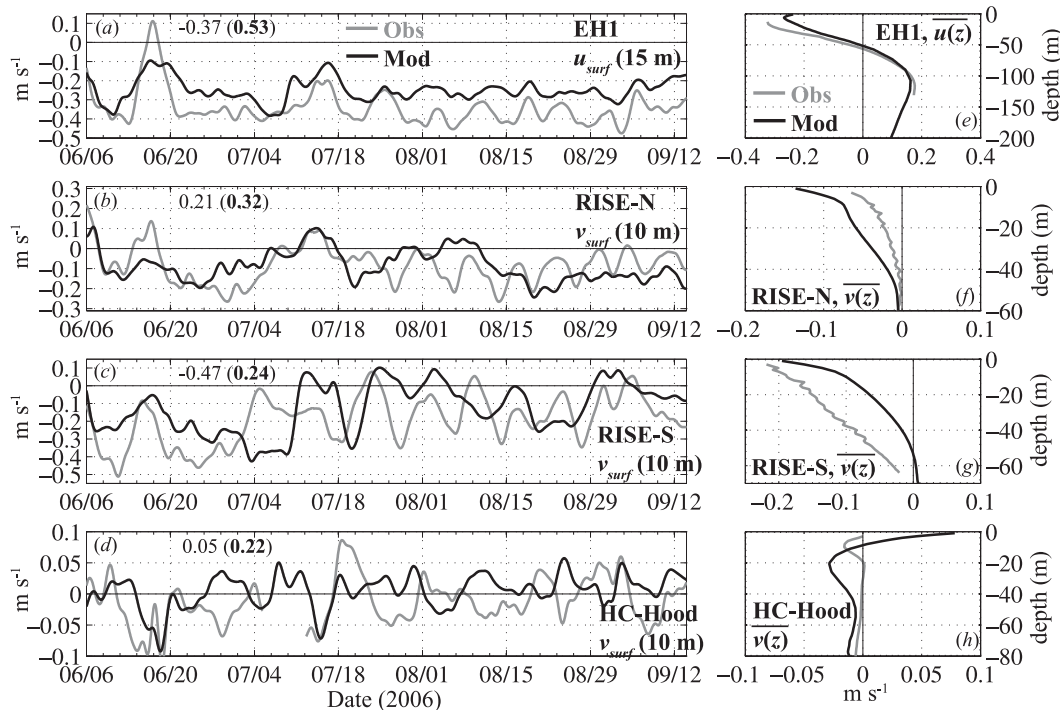


FIG. 9. (a)–(d) Observed (gray) and modeled (black) tidally averaged, near-surface velocity records taken at several mooring locations over a 3-month period in summer 2006. At EH1, u_{surf} is shown, whereas v_{surf} is shown for all others. Note the scale changes between each panel. Skill scores SS are listed with R^2 correlation coefficients in parentheses (boldface if significant at the 95% level). (e)–(h) Observed (gray) and modeled (black) mean velocity profiles as a function of depth over the length of the observational record for the same velocity components shown in (a)–(d). Note the depth and velocity scales change between each panel.

TABLE 4. Skill scores SS and correlation coefficients R^2 for comparisons between moored ADCP records and ROMS model output at various locations. The R^2 values and SS > 0 that are significant at the 95% are listed in boldface.

Station	u_{surf}	v_{surf}	v_{deep}	u_{ave}	v_{ave}
EH1	-0.37 (0.53)	-0.26 (0.10)	-2.4* (0.43)**	0.89 (0.90)	0.09 (0.38)
EH2	0.04 (0.20)	-0.25 (0.44)	0.51 (0.58)	0.01 (0.18)	-0.88 (0.37)
RISE-N	-0.68* (0.05)	0.21 (0.32)	0.25 (0.27)	-0.44* (0.23)	-0.16* (0.25)
RISE-C	-0.96* (0.02)	-0.67 (0.33)	-0.98 (0.16)	-1.6* (0.01)	-2.8 (0.24)
RISE-S	-1.1* (0.01)	-0.47* (0.24)	0.29 (0.38)	-1.9* (0.0)	-0.09* (0.24)
HCN-Hood	-5.5* (0.04)	0.05 (0.22)	-0.5 (0.01)	-7.9* (0.48)	0.34 (0.64)

* Variance bias > mean bias in making SS < R^2 (in those cases with SS < 0).

** In the case of EH1, u_{deep} is used because the flow is primarily east-west.

of coastal upwelling? Babson et al. (2006) found that, for much of the sound, SJdF salinity was of greatest importance. To begin to answer these types of questions in the model, we first examine the exchange flow and salt flux patterns across the region.

a. Total exchange flow and salt flux

A simple way to examine the estuarine salt balance is to combine the conservation of salt and volume into the Knudsen relations,

$$-Q_{\text{in}} = \frac{S_{\text{out}}}{\delta S} Q_R + \frac{1}{\delta S} \frac{d}{dt} \int S dV \quad \text{and} \quad (4.1)$$

$$Q_{\text{out}} = \frac{S_{\text{in}}}{\delta S} Q_R + \frac{1}{\delta S} \frac{d}{dt} \int S dV, \quad (4.2)$$

where Q_{in} and Q_{out} are the volume fluxes of water into and out of the estuary, respectively, and Q_R is the freshwater flux. In this study, we define these volume fluxes by calculating the transport as a function of salinity $Q(S)$. Following the derivation by MacCready (2011),

$$Q(S) = \left\langle \int_{A_S} u dA \right\rangle, \quad (4.3)$$

where the velocity u across a section is integrated over the tidally varying area A_S , where the salinity is greater than S . Angled brackets indicate a tidal average. To calculate the volume flux over a limited salinity range, one can find the derivative $\partial Q/\partial S$, where positive $\partial Q/\partial S$ indicates flow out of the estuary. In practice, this means calculating the volume transport across a given section at every time step, binning those transports into a finite set of salinity classes, and then taking the tidal average of those transports. An example of $\partial Q/\partial S$ (Fig. 11) illustrates that it is akin to a histogram of transport in discrete salinity bins and is discussed in more detail below. Here, Q_{in} (Q_{out}) is then the sum of $\partial Q/\partial S$ over all the incoming (outgoing) water, and $\delta S = S_{\text{in}} - S_{\text{out}}$, where $S_{\text{in}} = F_{\text{in}}/Q_{\text{in}}$ and $S_{\text{out}} = F_{\text{out}}/Q_{\text{out}}$ are

the flux-weighted salinities of the in- and out-estuary transport. The salt fluxes are equal to

$$F_{\text{in}} \equiv \int S \left(\frac{\partial Q}{\partial S} \right) \Big|_{\text{in}} dS, \quad F_{\text{out}} \equiv \int S \left(\frac{\partial Q}{\partial S} \right) \Big|_{\text{out}} dS, \quad (4.4)$$

where the integrals are only over the salinity bins with incoming or outgoing volume transport.

The four terms Q_{in} , Q_{out} , S_{in} , and S_{out} will be collectively called the total exchange flow (TEF), because they intrinsically carry the full salt flux and make (4.1) and (4.2) exactly correct (MacCready 2011). In contrast, it is common to calculate the exchange flow using the tidally averaged velocity organized by spatial position on the cross section (Lerczak et al. 2006) instead of salinity. We will refer to this method as the ‘‘Eulerian’’ exchange flow, denoted by superscript Eu, because it depends fundamentally on position in the water column and is related to what fixed instruments would observe. The Eulerian terms do not include salt fluxes due to tidal correlations of transport and salinity, whereas the TEF terms do. A full derivation of the TEF terms and further comparison with the Eulerian decomposition is given in MacCready (2011).

Comparison of the exchange flow calculated from the two methods at AIN reveals significant differences

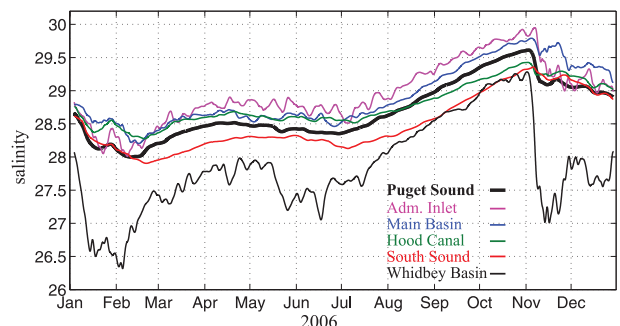


FIG. 10. Tidally averaged mean salinity of Puget Sound (thick black line) and its basins (thin colored lines), calculated from the numerical model over the year 2006.

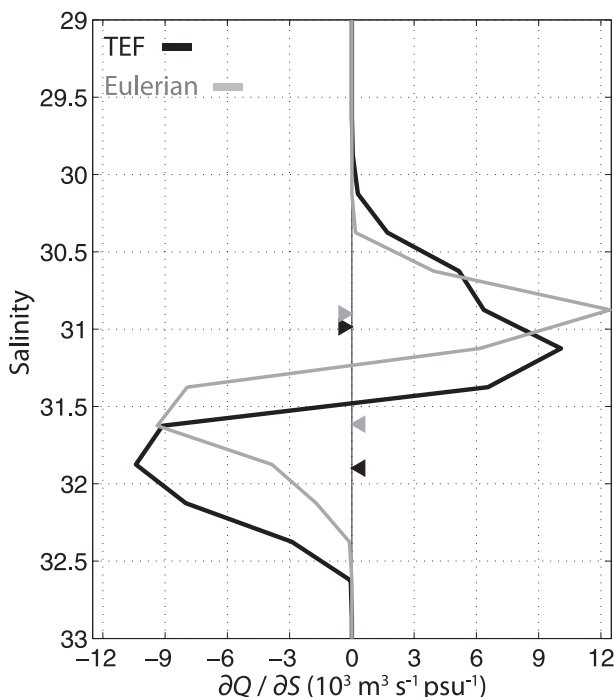


FIG. 11. Exchange flow as a function of salinity, $\partial Q/\partial S$, averaged over a spring–neap cycle in September 2006 at AIN. The exchange flow calculated using the TEF formulation (black) covers a wider range of salinity (triangles denote S_{in} and S_{out}) than the Eulerian estimate (gray).

(Fig. 11). Though the magnitudes of the transports are similar, the TEF spans a significantly wider range of salinities. Here, S_{in} is 31.9, whereas S_{in}^{Eu} is 31.6; S_{out} is similar to S_{out}^{Eu} (31 and 30.9, respectively) but includes contributions from both fresher and saltier salinity classes.

Figure 12 illustrates the range and variability of the annual average TEF terms across the Salish Sea, using the sections shown in Fig. 4. Changes in S_{in} and S_{out} between sections reflect water mass modification, because of either the addition of water with a different salinity or the presence of mixing processes. The incoming water from the coastal ocean changes little through the SJdF to the entrances of Puget Sound and the SoG (Fig. 12). This suggests that mixing is negligible along the SJdF, relative to the modification that happens at AIN and SoG. The outgoing waters from the SoG and Puget Sound have $S_{out} \sim 30.5$ but are significantly altered as they transit into the SJdF and exit into the coastal ocean at $S_{out} \sim 31.5$.

The largest modifications to S_{in} and S_{out} occur between basins. For example, S_{in} changes little across Main Basin from north to south, going from 31.1 to 30.8, whereas S_{out} actually increases, going from 29.4 to 30.2 because of the input of the Skagit and Snohomish River waters exiting Whidbey Basin. In general, though, both S_{in} and S_{out} decrease from the SJdF into Puget Sound

and the SoG (Fig. 12a). A fall off also occurs in $-Q_{in}$, decreasing from a maximum of $130 \times 10^3 \text{ m}^3 \text{ s}^{-1}$ at the entrance to the SJdF to $28 \times 10^3 \text{ m}^3 \text{ s}^{-1}$ at Admiralty Inlet and $83 \times 10^3 \text{ m}^3 \text{ s}^{-1}$ into the SoG.

The TEF-derived Q_{in} and Q_{out} have magnitudes much greater than the river discharge alone, expressed by the amplification factor $\alpha_r = Q_{in}/Q_r$. Here, α_r ranges from 10–40, except in the far reaches of Puget Sound, where Q_r gets small, and $\alpha_r \sim 130$ at Tacoma Narrows. These results are qualitatively consistent with those of Cokelet et al. (1991).

Although the annual average TEF highlights the general structure of the estuarine circulation in Puget Sound and the Salish Sea, it hides the rich time dependence hinted at in Fig. 10. Both Q_{out} and Q_{in} at AIN progressively get saltier from later summer into the fall, mimicking the variability in salt content (Fig. 13). When the storm season starts in November, Q_{out} freshens and increases initially because of the increased river discharge and then reverses for a short time period. On top of this seasonal variability, the TEF at AIN is modulated on spring–neap time scales, as can be seen from its diverging and converging values (Fig. 13a). During neap tides, Q_{out} decreases in salinity class and Q_{in} brings in saltier waters, whereas they converge toward similar salinities during spring tides. These patterns are explored in more detail for AIN in Fig. 14. During spring tides the salinity difference between inflowing and outflowing water generally decreases, consistent with the observations of Geyer and Cannon (1982). However the magnitude of the transport terms generally increases during springs, contrary to their findings. These results are not necessarily conflicting, because our transport terms include tidal fluxes, whereas those of Geyer and Cannon (1982) do not.

At the entrance to Whidbey Basin, Q_{out} shows a low-salinity maximum coincident with the peak river discharges from the Skagit and Snohomish rivers, which gradually taper off through the fall months. The fall storms intensify and freshen Q_{in} almost immediately, resulting in an export of fresh waters to the Triple Junction region of Puget Sound. This sudden export is the probable cause of the reversal seen in the exchange flow (Q_{out} is saltier than Q_{in}) at Admiralty Inlet (Fig. 13a) and Main Basin north (not shown). Babson et al. (2006) observed this fall reversal in their box model study as well, attributing it to a sign reversal of the surface salinity gradient between the two basins.

In the lower reaches of Hood Canal (Fig. 13c), the magnitude of the TEF decreases significantly, but many of the same time dependent features are found. For example, when the Skokomish River discharge increases during the fall months, the out-estuary flow freshens and intensifies. During the summer, though, the pattern is

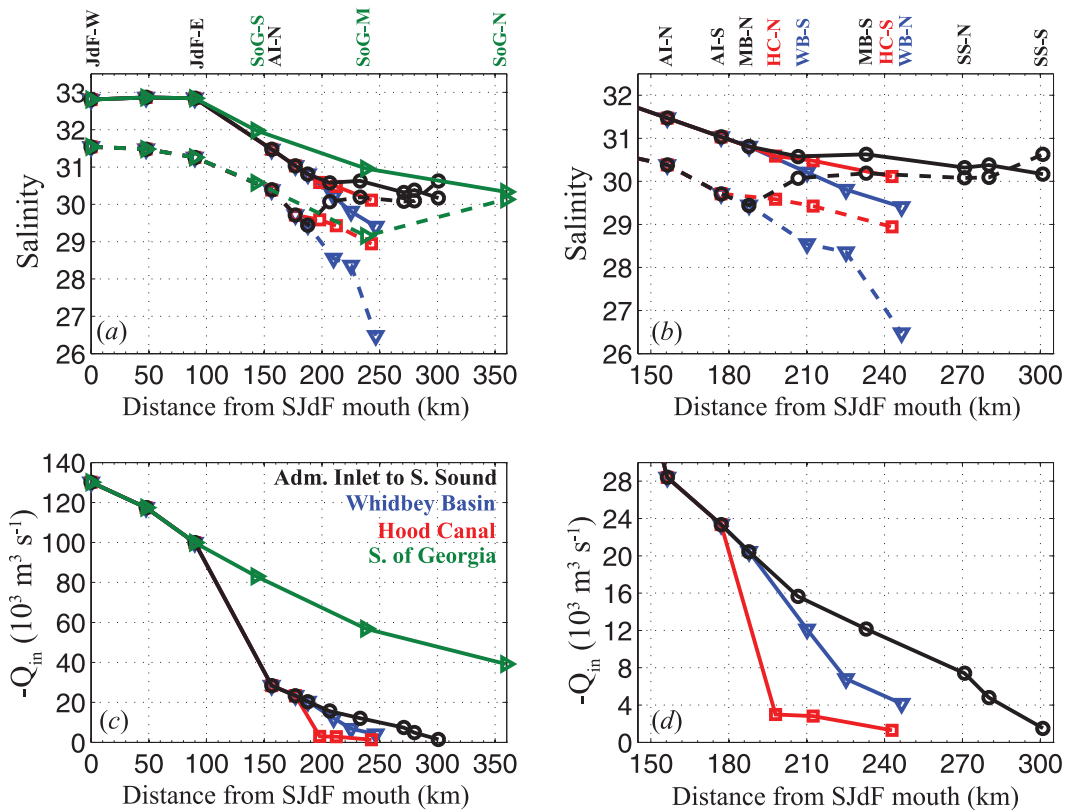


FIG. 12. (a) Annual average S_{in} (solid) and S_{out} (dashed) transport-weighted salinities vs distance from the mouth of the SJdF. Colors show the different paths along each basin of Puget Sound and the SoG. (b) As in (a), but zoomed in on the Puget Sound region. (c) As in (a), but for $-Q_{in}$, the in-estuary part of the TEF. (d) As in (c), but zoomed in on the Puget Sound region.

more complicated, with multiple layers of Q_{in} and Q_{out} ; the freshest waters are actually moving in estuary and then presumably entering Hood Canal from the north. Three-layered estuarine circulation has been observed in other parts of the sound (Edwards et al. 2007).

b. Admiralty Inlet salt flux variability

Although the TEF analysis presented above quantifies the actual flux of salt that is entering and exiting the estuary, it does not explicitly highlight what physical processes are controlling the salt content variability. The temporal variability in $\partial Q/\partial S$ (Fig. 13) and thus the salt flux can be correlated with various forcing mechanisms, and this section explores those relationships at Admiralty Inlet, where previous studies have investigated the exchange flow.

Important forcing mechanisms include the Skagit River discharge Q_r , the strength of the tides U_T , and north-south wind stress τ at the water surface. Here, U_T is calculated using the tidally averaged magnitude of the depth-averaged velocity. Increasing tidal velocities increase bottom stress and can lead to enhanced

mixing in regions with intense tidal currents; this enhanced mixing can feedback on the exchange flow and lead to changes in the net salt flux, $F_{net} = F_{in} + F_{out}$. The wind stress can directly influence the salt flux by accelerating the surface layer flow, causing compensating changes in F_{in} .

Decreasing U_T results in less tidal mixing during neap tides and an observed enhancement of the stratification and exchange flow (Geyer and Cannon 1982), which is supported by the negative correlation coefficients for F_{out} (Table 5). The correlation is strongest during the low-discharge summer months but is still significant in the annual average. However, our TEF results presented in Fig. 14 indicate that this correlation of high salt flux with neap tides must be mainly due to the changing stratification, because the volume transports are positively correlated with the tides. Interestingly, the influence of the river discharge is only significant with F_{net} . Wind forcing is significantly correlated to F_{out} but not F_{net} , indicating the northward winds at AIN tend to drive more exchange flow. Correlations for F_{in} were similar in magnitude but the opposite sign of the F_{out} results.

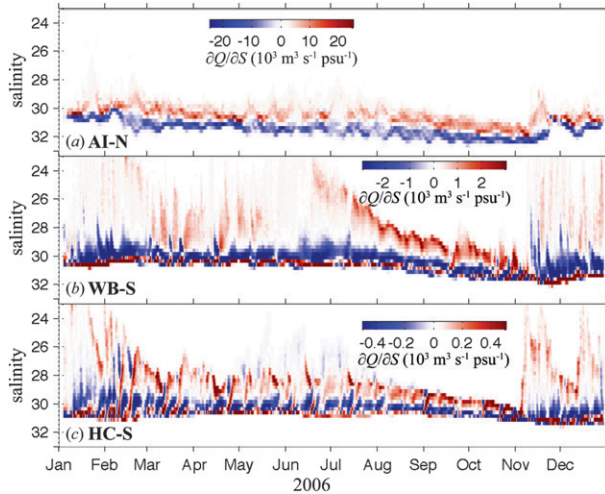


FIG. 13. (a) Tidally averaged exchange flow, $\partial Q/\partial S$ ($10^3 \text{ m}^3 \text{ s}^{-1} \text{ psu}^{-1}$), across the AIN north section. Here, $\partial Q/\partial S > 0$ indicates out-estuary flow. (b) As in (a), but for the Whidbey Basin south section. The axis limits stay constant, but note that the color scale changes. (c) As in (a), but for the Hood Canal south section. The axis limits stay constant, but note that the color scale changes.

c. Partitioning of Skagit River water

Another example of the utility of the TEF formalism comes in looking at the partitioning of the freshwater flux that can be used to quantify the distribution of different river sources to an estuary. For example, in Skagit Bay, Skagit River water can exit westward through DP or southward through Saratoga Passage (WBN). The distribution of river water here is also important, because it influences where sediment is carried and may impact how reversals in the Main Basin exchange flow are created as low-salinity waters exit Whidbey Basin (Babson et al. 2006).

The freshwater portion of the out-estuary transport Q_{FW} can be calculated simply once the total exchange flow is known by combining the Knudsen relations (4.1) and (4.2) with volume conservation,

$$Q_{FW} = \left(1 - \frac{S_{out}}{S_{in}}\right) Q_{out} - \frac{1}{S_{in}} \frac{d}{dt} \int_V S dV. \quad (4.5)$$

In (4.5), S_{in} is the flux-weighted salinity of the total incoming transport between DP and WBN and S is the mean salinity of the volume V defined between the sections.

The annual-mean Skagit River discharge is $470 \text{ m}^3 \text{ s}^{-1}$. Over an annual average, the storage term is negligible, and we find that $180 \text{ m}^3 \text{ s}^{-1}$ (38%) of the freshwater exits Skagit Bay through Deception Pass and $290 \text{ m}^3 \text{ s}^{-1}$ (62%) exits southward.

The fraction of Skagit River water passing through Deception Pass is highly variable throughout the year,

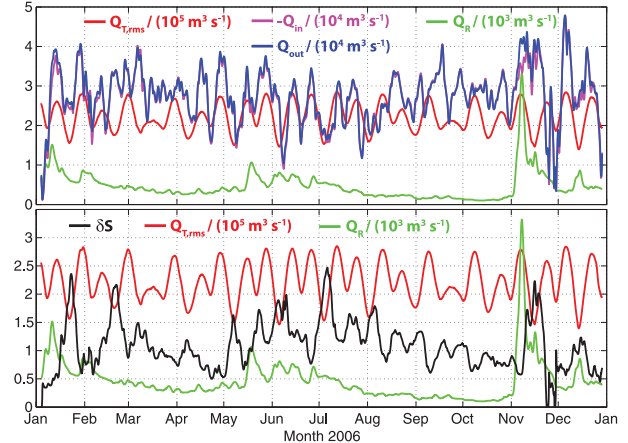


FIG. 14. Tidally averaged TEF terms at the AIN section, over the model year. The forcing terms are plotted as red (Q_{Trms} ; tides) and green (Q_r ; rivers), with units given in the legend. (top) The TEF exchange flow $Q_{in,out}$ and (bottom) the difference of flux-weighted salinities $\delta S = S_{in} - S_{out}$. Although δS tends to decrease during spring tides, the exchange flow increases.

though in the winter months it is generally larger in magnitude and positive (Fig. 15). During the summer, southward flow through WBN carries the majority of the freshwater out of Skagit Bay (Fig. 15b). Variability in Q_{FW} at DP is related to wind forcing, much like southward winds decreased F_{out} at AIN. Northward and westward winds are correlated with increased freshwater transport at DP, with R^2 of 0.65 (-0.61) between north-south wind stress (east-west wind stress) and Q_{FW} . This wind influence is consistent with previous detailed numerical simulations of the Skagit River Delta (Yang and Khangaonkar 2008).

d. Residence times in Puget Sound

The concept of residence time T_{res} is critical to understanding the functioning of an estuary, because it connects the physical circulation features with biologically important time scales. The strength of the residual circulation, quantified by the TEF, determines this residence time. Driven by the river flow alone, T_{res} would equal the river filling time, $T_{riv} = V/Q_r$, about 5 yr,

TABLE 5. Correlation coefficients at AIN between F_{out} and F_{net} against three forcing mechanisms: Skagit River discharge Q_r , tidal velocity U_T , and north-south wind stress τ . A negative correlation indicates that increases in Q_r , U_T , and τ weaken the respective salt flux term. Values significant at the 95% level are in boldface.

	Q_r	U_T	τ
F_{out}	-0.25	-0.41	0.41
F_{net}	0.70	-0.21	-0.15

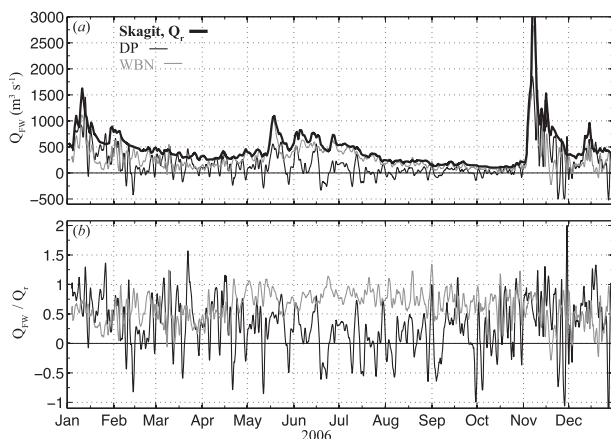


FIG. 15. (a) Components of the freshwater transport Q_{FW} ($\text{m}^3 \text{s}^{-1}$) in Skagit Bay including the inflowing river water (Q_r ; thick black line) and outgoing transport at DP (thin black line) and WBN north (thin gray line). (b) The outgoing freshwater transport Q_{FW} , normalized by the river discharge Q_r , at DP (thin black line) and WBN north (thin gray line).

where $V = 169 \text{ km}^3$ is the volume (Lavelle et al. 1988) and $Q_r = 36.5 \text{ km}^3 \text{ yr}^{-1}$. However, the exchange flow is amplified over the river discharge.

The simplest method to use in estimating estuarine residence times is a box model approach, which was done for Puget Sound in a study aimed at describing seasonal to interannual changes (Babson et al. 2006). More sophisticated techniques rely on high-resolution numerical model results. These include the age tracer method that was used, for example, in a study of Willapa Bay, Washington (Banas and Hickey 2005), or through repeated dye release experiments: for example, as done in the Hudson River (Warner et al. 2010).

In this study, we calculate saltwater residence times based on the box model approach to give order of magnitude estimates that are useful in characterizing the unique basins of Puget Sound. Following MacDonald (2006), we will use the fluxes averaged in salinity classes (TEF). The saltwater residence time is defined as

$$T_{\text{res}} = \int S dV / F_{\text{in}}, \quad (4.6)$$

where the integral is over each respective volume. Figure 16 shows T_{res} for Puget Sound landward of AIN and DP and four basins defined as landward of their most seaward section (e.g., HCN). These T_{res} are median values of the distribution calculated using tidally averaged values of each variable.

Puget Sound has a median T_{res} of 57 days (51–67 days represent the first and third quartiles, because all the distributions had positive skewness), much less than the 139 days estimated previously (Babson et al. 2006). To

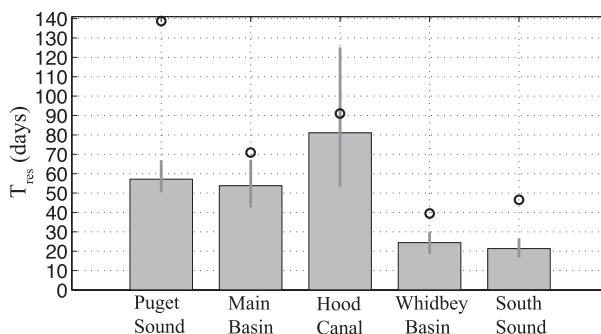


FIG. 16. Median saltwater residence times T_{res} (days) for Puget Sound and its four major basins, where each volume is defined in the text. The lines on each bar indicate the first and third quartile ranges of the T_{res} distribution, whereas open circles denote the Babson et al. (2006) estimates.

ensure a meaningful comparison between the two-layer box model and the present simulation, we recalculated the Babson et al. (2006) transports at each section, and then used those values to compute T_{res} for each volume under consideration. The discrepancy in T_{res} may be because the Babson et al. (2006) model appeared to overestimate the stratification at Admiralty Inlet, which leads to an underestimate of the exchange flow.

Hood Canal was found to have the longest $T_{\text{res}} \sim 81$ days (53–125 days), in line with the previous estimates for the region, with a high upper range that occurs primarily during the low-flow summer months. Overall, the residence times calculated here are shorter than those found previously.

5. Discussion

The three large estuarine systems that comprise the Salish Sea, Puget Sound, the SJdF, and the SoG are themselves composed of smaller estuarine basins, such as Hood Canal and Whidbey Basin, as well as individual river systems, such as the Fraser and Skagit Rivers. This is one of the reasons it has been difficult to classify Puget Sound as a specific type of estuary. Our model results, though, do support the notion that Puget Sound has many properties characteristic of partially mixed estuaries, including a vigorous exchange flow with $\alpha_r \gg 1$; an along-estuary salinity gradient; and variations in salt flux correlated to river discharge, winds, and the strength of the tides.

The steady Knudsen relation is a good approximation for the salt balance in Puget Sound. The salt flux terms are $O(10^6 \text{ kg s}^{-1})$, two orders of magnitude larger than the storage term, $O(10^4 \text{ kg s}^{-1})$. The slight differences in the salt flux terms do drive changes in the salt content of Puget Sound, but the system is in a near steady state over

a yearly cycle. Increases in salinity are delayed in South Sound and Whidbey Basin, relative to Admiralty Inlet, Hood Canal, and Main Basin. This suggests that the driver for the gain of salt is propagating in from outside Puget Sound and is not solely driven by decreasing river discharge, consistent with findings in Babson et al. (2006).

Assuming one could use theoretical scales derived for partially mixed estuaries in Puget Sound, we can estimate the length of the salt intrusion, $L > 1000$ km, which is much greater than the length of the sound itself (MacCready and Geyer 2010). Here, L is sensitive to the strength of tidal mixing, $L \propto U_T^{-1}$, but only depends weakly on river discharge, $L \propto Q_r^{-1/3}$, in classic estuarine theory (Hansen and Rattray 1965; MacCready and Geyer 2010). In contrast, the stratification and exchange flow theoretically vary only with changes in Q_r and bathymetry and do not depend upon U_T .

One reason for the mean S bias found in the model could be that L is too long because of not enough tidal energy flux into Puget Sound. This would increase L but not affect the stratification and exchange flow, which were more accurately simulated. To test this hypothesis, we calculated the flux of tidal energy, $F_{\text{tidal}} = \rho_0 g \zeta Q_{\text{net}}$, at each section, where ρ_0 is a constant background density (1023 kg m^{-3}), g is the acceleration due to gravity, ζ is the cross-sectionally averaged sea surface height, and $Q_{\text{net}} = Q_{\text{in}} + Q_{\text{out}}$ with no tidal averaging. Lavelle et al. (1988) calculated F_{tidal} in Puget Sound using an empirical tide model and found that 730 MW propagated into northern Admiralty Inlet. In this model, we find that $F_{\text{tidal}} \sim 310$ MW at AIN, or about 42% of the observed tidal energy flux. Most likely, this is due to not resolving the sharpness and number of bathymetric features that act as a drag on the tidal flow (Edwards et al. 2004; McCabe et al. 2006). Despite this discrepancy at Admiralty Inlet, the tidal energy fluxes calculated at the remaining Lavelle et al. (1988) sections inside Puget Sound are in closer agreement, differing by only 10% or less.

6. Conclusions and summary

This study examined the functioning of the estuarine systems that constitute the Salish Sea, with particular emphasis on Puget Sound. A numerical model has been developed that has moderate skill in hindcasting the circulation and water masses observed in the region. We find that the subtidal circulation of Puget Sound, the Strait of Juan de Fuca, and the Strait of Georgia, have properties that resemble partially mixed estuaries studied elsewhere. The magnitude of the total exchange flow drops off from ~ 0.1 Sv at the mouth of the SJdF to ~ 0.03 Sv at the entrance to Puget Sound. Coincident

with the change in exchange flow is a pronounced modification of the salinity of waters entering and exiting the Salish Sea. In particular, we find that the sill regions of Admiralty Inlet and the San Juan Islands are locations of intense buoyancy flux, with salinities changing dramatically across relatively short distances.

Temporal variations in salt flux are correlated with environmental conditions, such as river discharge, wind stress, and the strength of tidal currents. Our results are consistent with observed modulation of the stratification at Admiralty Inlet on spring–neap time scales because of variations in tidal mixing. In contrast, the strength of the exchange flow (as calculated in isohaline coordinates) increases during springs.

The calculation of volume fluxes in salinity classes was found to allow simpler and more accurate calculation of important properties of the system, including the overall structure of the exchange flow; the saltwater residence time; the freshwater flux out of Deception Pass; and the response of the Admiralty Inlet exchange flow to forcing by wind, rivers, and tides. The residence time calculation suggested that Puget Sound has a residence time of ~ 2 months, which is supported by the salt content variability on seasonal time scales. The model provides some evidence that the seasonal change in salt content within Puget Sound is driven externally via the Strait of Juan de Fuca rather than by variability in river discharge locally. However, a definitive answer to this question, along with others such as how much Columbia River water penetrates into the Salish Sea, is left to a future study.

Acknowledgments. Funding was provided by the State of Washington through the University of Washington Puget Sound Regional Synthesis Model (PRISM) project, and we thank M. Warner, J. Newton, and M. Kawase for leading the data collection part of PRISM. Additional support came from the National Science Foundation Grants 0849622 and 0751683 and the Vetlesen Foundation. This project benefited from many observational programs, but we especially thank B. Hickey for leading the RISE project and sharing the CTD data; E. Dever for the RISE mooring data; and B. Hickey for leading the ECOHAB PNW project, which is supported by the Coastal Ocean Program of the National Oceanic and Atmospheric Administration (NA09NOS4780180) and the National Science Foundation (OCE0942675). The Institute of Ocean Sciences in Canada and the Washington State Department of Ecology generously shared their data, including the Joint Effort to Monitor the Straits (JEMS) led by C. Maloy and J. Newton and cosponsored by Ecology and PRISM. J. Newton, M. Alford, A. Devol, and J. Mickett provided leadership

for the Hood Canal Dissolved Oxygen Program (HCDOP), funded through the U.S. Navy NAVSEA. D. Darr provided system administration, and C. Bassin helped archive data. Two anonymous reviewers provided comments that greatly improved the clarity and content of this manuscript.

REFERENCES

- Babson, A. L., M. Kawase, and P. MacCready, 2006: Seasonal and interannual variability in the circulation of Puget Sound, Washington: A box model study. *Atmos.–Ocean*, **44**, 29–45.
- Banas, N. S., and B. M. Hickey, 2005: Mapping exchange and residence time in a model of Willapa Bay, Washington, a branching, macrotidal estuary. *J. Geophys. Res.*, **110**, C11011, doi:10.1029/2005JC002950.
- Barron, C. N., A. B. Kara, P. J. Martin, R. C. Rhodes, and L. F. Smedstad, 2006: Formulation, implementation and examination of vertical coordinate choices in the global Navy Coastal Ocean Model (NCOM). *Ocean Modell.*, **11**, 347–375.
- , L. F. Smedstad, J. M. Dastugue, and O. M. Smedstad, 2007: Evaluation of ocean models using observed and simulated drifter trajectories: Impact of sea surface height on synthetic profiles for data assimilation. *J. Geophys. Res.*, **112**, C07019, doi:10.1029/2006JC003982.
- Beckmann, A., and D. B. Haidvogel, 1993: Numerical simulation of flow around a tall, isolated seamount. Part I: Problem formulation and model accuracy. *J. Phys. Oceanogr.*, **23**, 1736–1753.
- Canuto, V. M., A. Howard, Y. Cheng, and M. S. Dubovikov, 2001: Ocean turbulence. Part I: One-point closure model—Momentum and heat vertical diffusivities. *J. Phys. Oceanogr.*, **31**, 1413–1426.
- Chapman, D. C., 1985: Numerical treatment of cross-shelf open boundaries in a barotropic coastal ocean model. *J. Phys. Oceanogr.*, **15**, 1060–1075.
- Cokelet, E. D., R. J. Stewart, and C. C. Ebbesmeyer, 1991: Concentrations and ages of conservative pollutants in Puget Sound. *Puget Sound Research Proceedings*, T. W. Ransom, Ed., Puget Sound Water Quality Authority, 99–108.
- Edwards, K. A., P. MacCready, J. N. Moum, G. Pawlak, J. M. Klymak, and A. Perlin, 2004: Form drag and mixing due to tidal flow past a sharp point. *J. Phys. Oceanogr.*, **34**, 1297–1312.
- , M. Kawase, and C. P. Sarason, 2007: Circulation in Carr Inlet, Puget Sound, during spring 2003. *Estuaries Coasts*, **6**, 945–958.
- Egbert, G. D., and S. Y. Erofeeva, 2002: Efficient inverse modeling of barotropic ocean tides. *J. Atmos. Oceanic Technol.*, **19**, 183–204.
- Emery, W. J., and R. E. Thomson, 1997: *Data Analysis Methods in Physical Oceanography*. Pergamon Press, 634 pp.
- Fairall, C. W., E. F. Bradley, D. P. Rogers, J. B. Edson, and G. S. Young, 1996: Bulk parameterization of air-sea fluxes for Tropical Ocean-Global Atmosphere Coupled-Ocean Atmosphere Response Experiment. *J. Geophys. Res.*, **101**, 3747–3764.
- Finlayson, D. P., 2005: Combined bathymetry and topography of the Puget Lowland, Washington State. University of Washington School of Oceanography. [Available online at <http://www.ocean.washington.edu/data/pugetsound/psdem2005.html>.]
- Flather, R. A., 1976: A tidal model of the northwest European continental shelf. *Mem. Soc. Roy. Sci. Liege*, **10**, 141–164.
- Frisch, A. S., J. Holbrook, and A. B. Ages, 1981: Observations of a summertime reversal in circulation in the Strait of Juan de Fuca. *J. Geophys. Res.*, **86**, 2044–2048.
- García-Berdeal, I., B. M. Hickey, and M. Kawase, 2002: Influence of wind stress and ambient flow on a high discharge river plume. *J. Geophys. Res.*, **107**, 3130, doi:10.1029/2001JC000932.
- Geyer, W. R., and G. A. Cannon, 1982: Sill processes related to deep water renewal in a fjord. *J. Geophys. Res.*, **87**, 7985–7996.
- Godin, G., 1991: The analysis of tides and currents (review). *Progress in Tidal Hydrodynamics*, B. B. Parker, Ed., John Wiley, 675–709.
- Gregg, M. C., and L. J. Pratt, 2010: Flow and hydraulics near the sill of Hood Canal, a strongly sheared, continuously stratified fjord. *J. Phys. Oceanogr.*, **40**, 1087–1105.
- Griffin, D. A., and P. H. LeBlond, 1990: Estuary/ocean exchange controlled by spring-neap tidal mixing. *Estuarine Coastal Shelf Sci.*, **30**, 275–297.
- Haney, R. L., 1991: On the pressure gradient force over steep topography in sigma coordinate ocean models. *J. Phys. Oceanogr.*, **21**, 610–619.
- Hansen, D. V., and M. Rattray, 1965: Gravitational circulation in straits and estuaries. *J. Mar. Res.*, **23**, 104–122.
- Haugerud, R. A., 2000: Digital elevation model (DEM) of Cascadia, latitude 39N–53N, longitude 116W–133W. U.S. Geological Survey Report. [Available online at <http://geopubs.wr.usgs.gov/open-file/of99-369/>.]
- Hickey, B., R. McCabe, S. Geier, E. Dever, and N. Kachel, 2009: Three interacting freshwater plumes in the northern California Current System. *J. Geophys. Res.*, **114**, C00B03, doi:10.1029/2008JC004907.
- , and Coauthors, 2010: River influences on shelf ecosystems: Introduction and synthesis. *J. Geophys. Res.*, **115**, C00B17, doi:10.1029/2009JC005452.
- Labrecque, M. A., R. E. Thomson, M. Stacey, and J. Buckley, 1994: Residual currents in Juan de Fuca Strait. *Atmos.–Ocean*, **37**, 1–19.
- Lavelle, J. W., H. O. Mojfield, E. Lempriere-Doggett, G. A. Cannon, D. J. Pashinski, E. D. Cokelet, L. Lytle, and S. Gill, 1988: A multiple connected channel model of tides and tidal currents in Puget Sound, Washington, and a comparison with updated observations. NOAA Tech. Memo. ERL PMEL-84, 108 pp.
- Lerczak, J. A., W. R. Geyer, and R. J. Chant, 2006: Mechanisms driving the time-dependent salt flux in a partially stratified estuary. *J. Phys. Oceanogr.*, **36**, 2296–2311.
- Liu, Y., P. MacCready, and B. M. Hickey, 2009a: Columbia River plume patterns in summer 2004 as revealed by a hindcast coastal ocean circulation model. *Geophys. Res. Lett.*, **36**, L02601, doi:10.1029/2008GL036447.
- , —, —, E. P. Dever, P. M. Kosro, and N. S. Banas, 2009b: Evaluation of coastal ocean circulation model for the Columbia River plume in summer 2004. *J. Geophys. Res.*, **114**, C00B04, doi:10.1029/2008JC004929.
- MacCready, P., 2011: Calculating estuarine exchange flow using isohaline coordinates. *J. Phys. Oceanogr.*, **41**, 1116–1124.
- , and W. R. Geyer, 2010: Advances in estuarine physics. *Annu. Rev. Mar. Sci.*, **2**, 35–58.
- , N. S. Banas, B. M. Hickey, E. P. Dever, and Y. Liu, 2009: A model study of tide- and wind-induced mixing in the Columbia River estuary and plume. *Cont. Shelf Res.*, **29**, 278–291.
- MacDonald, D. G., 2006: Estimating an estuarine mixing and exchange ratio from boundary data with application to Mt. Hope Bay (Massachusetts/Rhode Island). *Estuarine Coastal Shelf Sci.*, **70**, 326–332.
- Mass, C. F., and Coauthors, 2003: Regional environmental prediction over the Pacific Northwest. *Bull. Amer. Meteor. Soc.*, **84**, 1353–1366.

- Masson, D., and P. F. Cummins, 2000: Fortnightly modulation of the estuarine circulation in Juan de Fuca Strait. *J. Mar. Res.*, **58**, 439–463.
- McCabe, R., P. MacCready, and G. Pawlak, 2006: Form drag due to flow separation at a headland. *J. Phys. Oceanogr.*, **36**, 2136–2152.
- Mojfeld, H. O., and L. H. Larsen, 1984: Tides and tidal currents of the inland waters of western Washington. NOAA/Pacific Marine Environmental Laboratory Tech. Memo. ERL PMEL-56, 64 pp.
- Moore, S. K., N. J. Mantua, J. P. Kellogg, and J. A. Newton, 2008: Local and large-scale climate forcing of Puget Sound oceanographic properties on seasonal to interdecadal timescales. *Limnol. Oceanogr.*, **53**, 1746–1758.
- Murphy, A. H., 1988: Skill scores based on the mean square error and their relationships to the correlation coefficient. *Mon. Wea. Rev.*, **116**, 2417–2424.
- Newton, J., C. Bassin, A. Devol, M. Kawase, W. Ruef, M. Warner, D. Hannafous, R. Rose, 2007: Hypoxia in Hood Canal: An overview of status and contributing factors. *Proc. Puget Sound Georgia Basin Research Conf.*, Vancouver, BC, Canada, Puget Sound Partnership, 9A.
- Oke, P. R., and Coauthors, 2002: A modeling study of the three-dimensional continental shelf circulation off Oregon. Part I: Model–data comparisons. *J. Phys. Oceanogr.*, **32**, 1360–1382.
- Pawlowicz, R., R. Beardsley, and S. Lentz, 2002: Classical tidal harmonic analysis including error estimates in MATLAB using T_TIDE. *Comput. Geosci.*, **28**, 929–937.
- Ralston, D. K., W. R. Geyer, and J. A. Lerczak, 2010: Structure, variability, and salt flux in a strongly forced salt wedge estuary. *J. Geophys. Res.*, **115**, C06005, doi:10.1029/2009JC005806.
- Seim, H. E., and M. C. Gregg, 1997: The importance of aspiration and channel curvature in producing strong vertical mixing over a sill. *J. Geophys. Res.*, **102**, 3451–3472.
- Smith, W. H. F., and D. T. Sandwell, 1997: Global seafloor topography from satellite altimetry and ship depth soundings. *Science*, **277**, 1957–1962.
- Thomson, R. E., S. F. Mihály, and E. A. Kulikov, 2007: Estuarine versus transient flow regimes in Juan de Fuca Strait. *J. Geophys. Res.*, **112**, 09022, doi:10.1029/2006JC003925.
- Tinis, S. W., R. E. Thomson, C. F. Mass, and B. M. Hickey, 2006: Comparison of MM5 and meteorological buoy winds from British Columbia to northern California. *Atmos.–Ocean*, **44**, 65–81.
- Umlauf, L., and H. Burchard, 2003: A generic length-scale equation for geophysical turbulence models. *J. Mar. Res.*, **61**, 235–265.
- Warner, J. C., W. R. Geyer, and J. A. Lerczak, 2005: Numerical modeling of an estuary: A comprehensive skill assessment. *J. Geophys. Res.*, **110**, C05001, doi:10.1029/2004JC002691.
- , —, and H. G. Arango, 2010: Using a composite grid approach in a complex coastal domain to estimate estuarine residence time. *Comput. Geosci.*, **36**, 921–935, doi:10.1016/j.cageo.2009.11.008.
- Wilkin, J. L., 2006: The summertime heat budget and circulation of southeast New England shelf waters. *J. Phys. Oceanogr.*, **36**, 1997–2011.
- Willmott, C. J., 1981: On the validation of models. *Phys. Geogr.*, **2**, 184–194.
- Yang, Z., and T. Khangaonkar, 2008: Modeling tidal circulation and stratification in Skagit River estuary using an unstructured grid ocean model. *Ocean Modell.*, **28**, 34–49, doi:10.1016/j.ocemod.2008.07.004.
- Zhang, W. G., J. L. Wilkin, and R. J. Chant, 2009: Modeling the pathways and mean dynamics of river plume dispersal in the New York Bight. *J. Phys. Oceanogr.*, **39**, 1167–1183.